PROCEEDINGS OF SCIENCE

# Ray-Tracing in Relativistic Magnetohydrodynamic Jet Simulations: A Polarimetric Study

**Joana Kramer**[a,*] **and Nicholas MacDonald**[a]

[a] *Max Planck Institute for Radio Astronomy, Auf dem Huegel 69, Bonn, Germany*

*E-mail:* jkramer@mpifr-bonn.mpg.de, nmacdona@mpifr-bonn.mpg.de

The jets emanating from the centers of active galactic nuclei (AGNs) are among the most energetic objects in the universe. Investigations on how the morphology of the jet's synchrotron emission depends on the magnetic nature of the jet's relativistic plasma are fundamental to the comparison between numerical simulations and the observed polarization of the jet. Through the use of 3D relativistic magnetohydrodynamic (RMHD) jet simulations (computed using the PLUTO code) we study how the jet's synchrotron emission depends upon the morphology of the jet's magnetic field structure. Through the application of polarized radiative transfer and ray-tracing (via the RADMC-3D code) we create synthetic radio maps of the jet's total intensity as well as the linearly and circularly polarized intensity for each magnetic field jet simulation. In particular, we create synthetic ray-traced images of the jet's polarized synchrotron emission when the jet carries a predominantly poloidal, helical, and toroidal magnetic field. We also explore several scaling relations in which the underlying electron power-law distribution is set proportional to: (i) the jet's thermal plasma density, (ii) the jet's internal energy density, and (iii) the jet's magnetic energy density. Magnetic field morphology within the jet has a clear effect on the jet's resultant synchrotron emission. In particular, a toroidal field results in an edge-brightened jet whereas a poloidal field, in contrast, highlights the jet's central recollimation shock. Also, the circularly polarized emission clearly exhibits two signs in the toroidal field case whereas only one sign is visible in the poloidal jet.

*** *European VLBI Network Mini-Symposium and Users' Meeting (EVN2021)* ***
*** *12-14 July, 2021* ***
*** *Online* ***

*Speaker





PoS(EVN2021)025

## 1. Introduction

Theoretical models of AGN jets postulate that the jet plasma is likely magnetized with a large-scale helical morphology related to the launching of the jet by the rotation of the central black hole and accretion disk [2, 3, 10]. Recent observational evidence indicates that a large fraction of parsec-scale jets do indeed exhibit polarization signatures of helical magnetic field components. This is based on the detection of statistically significant transverse Faraday rotation measure (RM) gradients across the jet on parsec scales [7].

We set about carrying out a systematic study of how the fractional levels and morphology of both linearly and circularly polarized synchrotron emission depend on the underlying magnetic field morphology of the jet as well as various fluid scalings for the underlying electron power-law distribution. This study is executed with fully 3D relativistic magnetohydrodynamic (RMHD) jet simulations to conduct full Stokes polarized radiative transfer via ray-tracing [14].

RMHD simulations are unable to reproduce the kinetic scale physics of the jet (i.e., self-consistently generating the non-thermal distribution of electrons responsible for the observed synchrotron emission). We therefore rely on a purely macroscopic model of the jet that simulates the large scale dynamics of the thermal plasma within the jet flow. We explore various emission *recipes* for mapping from the thermal fluid variables to the non-thermal distribution of electrons [see, e.g., 22]. This mapping is carried out as a post-process step. In particular, we apply three scaling relations in which the non-thermal distribution of electrons is assumed to be proportional to the plasma's: *(i)* density, *(ii)* thermal pressure, and *(iii)* magnetic energy density. We also examine the effect that different magnetic field morphologies within the jet (namely; poloidal, helical, and toroidal) have on the dynamics of the jet as well as the resultant polarized emission.

## 2. Numerical Methods

In this section we briefly outline the numerical scaling relations used to generate synchrotron emission [4, 14, 18, 22]. We shortly introduce the RMHD module of the *PLUTO* code which forms the base for our simulation. Further, the physical scaling from *PLUTO*'s dimensional grid units requires the definition of fundamental units, i.e., velocity, length, and density. Additionally, we need to account for the non-thermal (micro) quantities by mapping these from the thermal (macro) fluid variables [4, 14].

### 2.1 Principles of the Relativistic Magnetohydrodynamics in the *PLUTO* Code

To model magnetized fluid flows, the *PLUTO* code integrates a system of conservation laws which can be expressed in general as:

$$\partial_t U^k + \sum_{i\in\{x,y,z\}} \partial_i T^{ik} = 0, \tag{1}$$

where $U^k$ is a state vector of $k$ conservative quantities and $T^{ik}$ is a rank 2 tensor. Moreover, $\partial_i$ is the four-gradient. The explicit form depends on the physical module selected within the code.

*PLUTO* solves a time-dependent non-linear system of special relativistic conservation laws, which in general have the form of Eq. 1. To account for the motion of an ideal relativistic magnetized

fluid, i.e., in relativistic magnetohydrodynamics, mass and energy-momentum are conserved. The solution to the specified problem of relativistic magnetohydrodynamics and therefore the conservative variables and respective fluxes for RMHD can be found in [14, 17].

### 2.2 Mapping the Non-Thermal onto the Thermal

The *PLUTO* simulations are computed in dimensionless grid units, therefore, the thermal quantities of the RMHD jet flow must be properly scaled into physical units as a post process step.[1]

An additional scaling relation is required in order to model the resultant non-thermal jet emission from our numerical simulations. The non-thermal quantities (i.e., electron number density and power-law energy cutoff) are inferred from the scaled thermal fluid variables of the simulation (i.e., plasma density, pressure, and magnetic field). This thermal to non-thermal mapping of our 3D RMHD jet simulations is used in the calculation of synchrotron emission maps. In particular, we initially assume an energy distribution of non-thermal relativistic electrons (NTEs) $n_e$ which follows a global power law distribution [see 4]. To solve for the unknowns of the electron power-law (i.e., lower energy power-law cutoff and normalization constant) we map the total number density of non-thermal electrons (NTEs) onto the thermal fluid variables [similar to 4].

For our ray-tracing calculations we then use the *RADMC-3D* code. The code reads in *PLUTO* output files that have been scaled into physical units. *RADMC-3D* produces 2D Fits images containing full Stokes polarization maps. The radiative transfer is implemented in our plasma simulations through the use of transport coefficients governing synchrotron absorption, synchrotron emissivity, Faraday rotation, and Faraday conversion (for a detailed description of the transfer matrix see [16]).

## 3. Magnetic Field Morphology Study

### 3.1 Magnetic Field Prescriptions

We study the impact that different magnetic field morphologies (i.e., poloidal, toroidal, and helical) within the 3D rotatable, non-axisymmetric jet have on the emitted polarized synchrotron radiation. To produce different magnetic field morphologies we implement (in Cartesian coordinates) expressions for the poloidal and toroidal components of the jet's magnetic field at the jet injection point (i.e., the jet orifice) in our simulations equivalent to Nishikawa et al. [19].

Figure 1 illustrates the three different simulated magnetic field morphologies within the jet (from left to right: poloidal, helical, toroidal). Here, the poloidal magnetic field vectors are aligned along the jet's axis (i.e., the $z$-direction) while the vectors for the toroidal components are predominantly perpendicular to the jet axis. The helical magnetic field vectors are rotated about $\sim 45^\circ$ in the jet's direction.

### 3.2 Imaging Pipeline

Figure 2 presents a summary of the various steps in our synthetic imaging pipeline. In particular, we are interested in studying the polarized properties of the jet's recollimation shock.

[1]The physical scaling of our RMHD jet simulations requires the definition of three fundamental units. For further details see the *PLUTO* Code (http://plutocode.ph.unito.it)

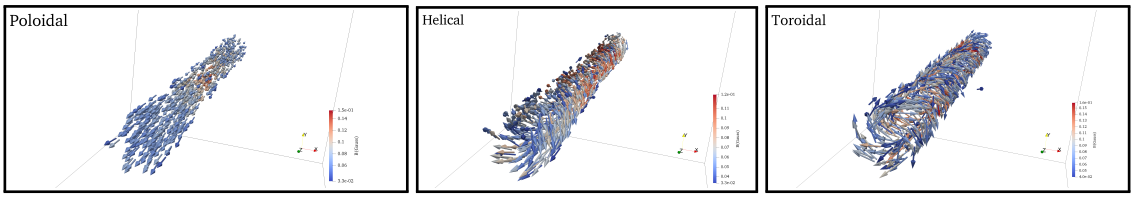


**Figure 1:** Illustration of the three different magnetic field morphologies within the 3D RMHD jet simulations. The jet is streaming in $z$-direction. The vectors represent the magnetic field strength (and orientation) in gauss (see the color bar) within each plasma cell. From left to right: poloidal, helical, and toroidal magnetic field morphologies.

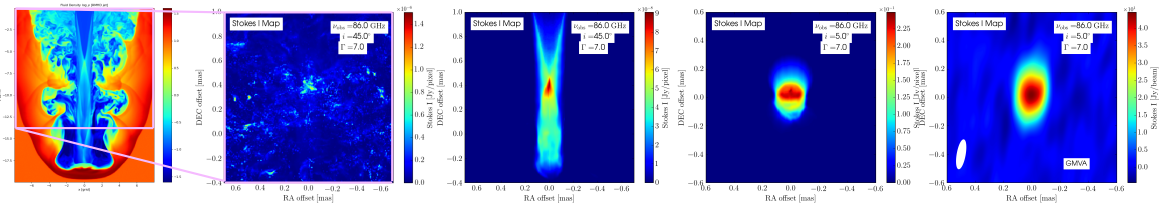


$(a)$ $(b)$ $(c)$ $(d)$ $(e)$

**Figure 2:** From left to right - a demonstration of our synthetic imaging pipeline: panel (a) starts with a 2D cut through our 3D RMHD jet colored by thermal density. Panels (b) through (e) are zoomed into an unobscured region of the jet's standing shock (demarcated with a purple box in panel (a)) and show: (b) the ray-traced synchrotron emission without the use of a jet tracer, (c) the ray-traced synchrotron emission with the use of a jet tracer to exclude the ambient medium, (d) the same simulation epoch but rotated to a viewing angle of $i = 5^\circ$, and (e) the ray-traced image convolved with a Gaussian beam indicative of the resolution of the GMVA and with a Gaussian noise floor (to mimic array sensitivity) of $10^{-1}$ Jy/beam.

We image an intermediate epoch of each jet simulation, i.e., when the jet's hot spot/terminal shock has not propagated off the grid yet. Through the use of a jet tracer we extract the region of plasma around the standing shock (demarcated with a purple box in the first panel of Fig. 2) in order to yield an unobscured view of the jet's central spine thus allowing us to image directly the jet flow upstream of the termination shock. These initial images were created using the poloidal magnetic field simulation. Panel (a) in Fig. 2 shows a 2D slice through the 3D jet simulation and displays the jet's density in dimensionless grid units. Panels (b)/(c) illustrate the zoomed-in ray-traced total intensity maps of the resulting synchrotron emission when the jet is resolved without/with the use of a jet tracer. The jet is viewed at an angle to the jet-axis of $i = 45^\circ$ and propagates from top to bottom. In the absence of radiative cooling (i.e., synchrotron losses) and larger simulation sizes we remove the bow shock from our ray-tracing calculations arbitrarily. Panel (d) displays the same snap-shot but rotated to a viewing angle of $i = 5^\circ$. Finally, panel (e) is convolved with a Gaussian beam, i.e., indicative of the resolution of the Global mm VLBI Array (GMVA), and with an added Gaussian noise floor (to mimic array sensitivity) of $10^{-1}$ Jy/beam. These final images show a bright radio core associated with the standing shock in our simulations. In all our RMHD jet simulations (in which each computational box consists of $320 \times 320 \times 400$ zones) we choose to view the source at a luminosity distance of 100 Mpc. The individual scaled cell size is 0.004 pc. All images in this proceedings are generated at an observing frequency of $\nu_{\rm obs} = 86$ GHz.

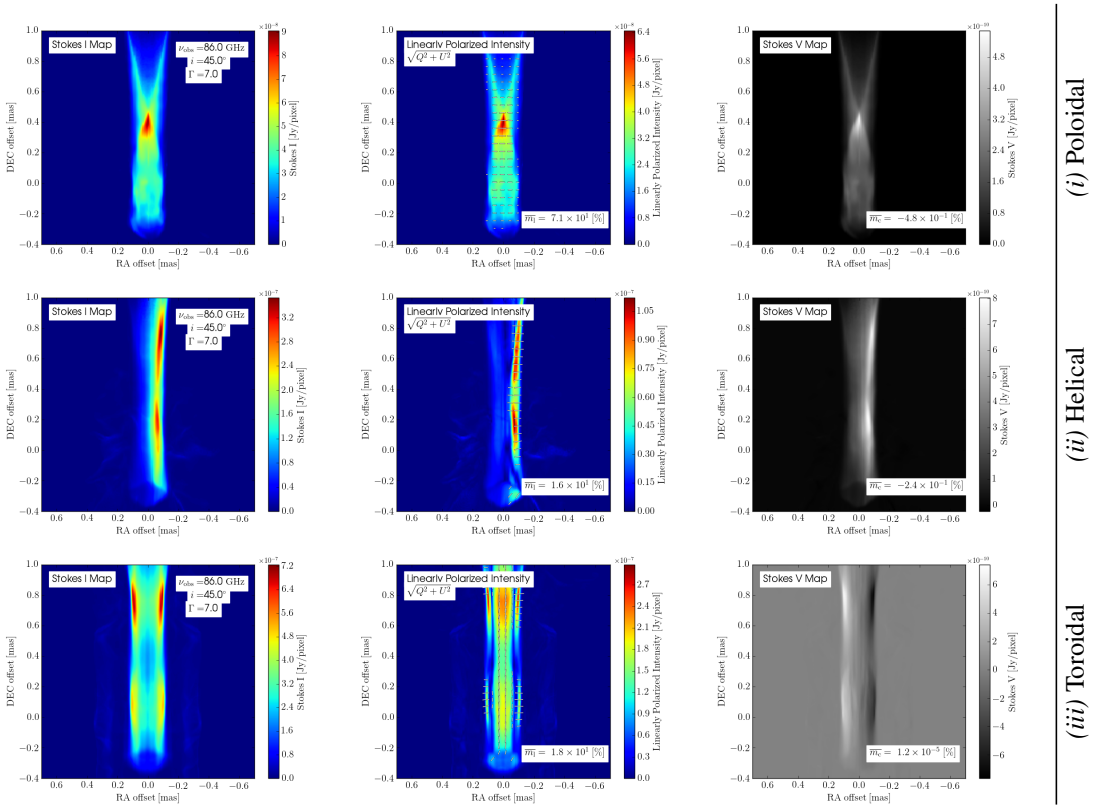


**Figure 3:** Ray-traced images of our jet propagating from top to bottom in total intensity (left column), in linearly polarized intensity (middle column), and circular polarization (right column). The pictures illustrate similar epochs in the jet's evolution of each 3D RMHD simulation at 86 GHz. The jet carries a purely poloidal magnetic field (top row), a helical magnetic field (middle row), and a purely toroidal magnetic field (bottom row). Integrated values of the fractional linear and circular polarization are listed to the lower right in the middle and right columns. The purely toroidal field jet appears edge-brightened in contrast to the poloidal jet which is brightest along the spine.

## 4. Results

We visualize the polarized synchrotron emission of the jet for three different magnetic field morphologies, i.e., purely poloidal, helical, and purely toroidal. To begin with, the images in Fig. 3 show the total intensity of the jet's emission in the left column, the linearly polarized intensity ($\equiv \sqrt{Q^2+U^2}$ ) including electric vector position angles (EVPAs, $\chi \equiv 0.5 \arctan[U/Q]$ ) in the middle column and the circular polarization in the right column. Moreover, the different rows represent the three magnetic field morphologies introduced in Section 3.1. The top row depicts the poloidal magnetic field, the middle row the helical field, and the bottom row the purely toroidal magnetic field. All ray-traced images are viewed at 45° to the jet-axis illustrated in Fig. 3.

We can see that the emission for the purely poloidal magnetic field is concentrated in the inner part of the jet, and is brightest within the standing recollimation shock. The EVPAs, shown as white line segments in the middle column of Fig. 3, are predominantly perpendicular to the magnetic field orientation, in the ideal case. As the poloidal field is streaming in the direction of the jet the EVPAs accurately convey the field orientation within our simulations. In contrast, the EVPA orientation in

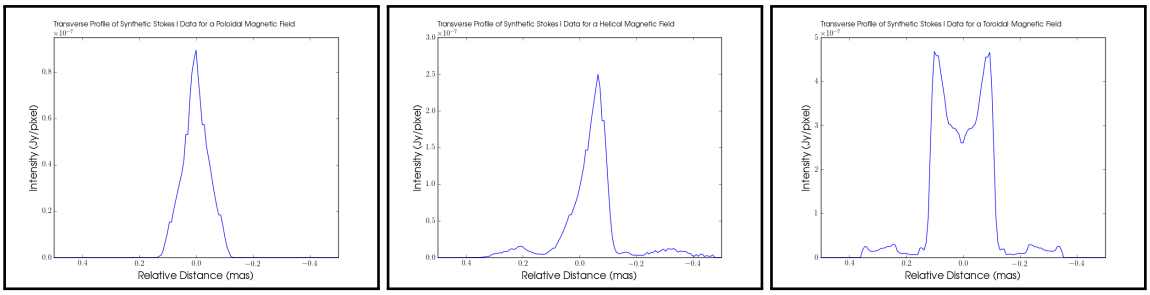


**Figure 4:** Illustration of the transverse profile (total intensity in Jansky/pixel vs relative distance in mas) for three different magnetic field morphologies (left/middle/right panel corresponding to poloidal/helical/toroidal) within the 3D RMHD jet simulations. A symmetrical shape for the edges of the jet is observed for the toroidal magnetic field. A single maximum in total intensity, as expected, exhibits the purely poloidal magnetic field configuration.

the toroidal magnetic field simulations exhibits a bi-modal pattern with distinct alignments in the jet's spine and the jet's sheath.

The toroidal magnetic field (bottom row of Fig. 3), clearly produces emission that is centered along the edges of the jet, and an edge-brightened jet morphology is seen both in total intensity and polarization In addition, we can see both positive and negative circular polarization highlighting the changing orientation of the jet's magnetic field with respect to our line-of-sight.

The helical magnetic field, illustrated in the middle row in Fig. 3, exhibits a mixture of the emission/polarization morphologies present in the toroidal/poloidal cases. The emission is concentrated on the right side of the relativistic jet which stresses the structure of the helical magnetic field lines.

In Fig. 4 we plot transverse profiles (total Intensity [Jy/pixel] vs. relative distance from the jet's central axis in mas) for the poloidal (left), helical (middle), and toroidal (right) magnetic field configurations. The profile of our synthetic stokes I data shows a double peaked profile for the edge-brightened toroidal magnetic field jet and a clear central peaked profile for the poloidal magnetic field configuration in the RMHD jet.

Figure 5 shows similar synthetic polarized synchrotron emission maps to those presented in Fig. 3 while the inclination changed to 5 degrees. The image is structured as before: the total intensity of the jet's emission in the left column, the linearly polarized intensity including EVPAs in the middle column and the circular polarization in the right column. The different rows represent the three magnetic field morphologies. The top row depicts the purely poloidal magnetic field, the middle one the helical field, and the bottom one the purely toroidal magnetic field.

In total intensity the poloidal field case exhibits a bright central radio core whereas, in contrast, the helical and toroidal field cases exhibit emission peaks offset from the central shock. Also, the helical and toroidal field cases exhibit two signs in circular polarization whereas the poloidal field case exhibits only one. In all cases, the linear polarized emission peaks are offset from the total intensity peaks which is commonly seen in blazars.

*Here, the most striking result are that* (i) *Fig. 3 demonstrates that resolved circular polarization imaging of relativistic jets has the potential to distinguish between a purely poloidal or purely*

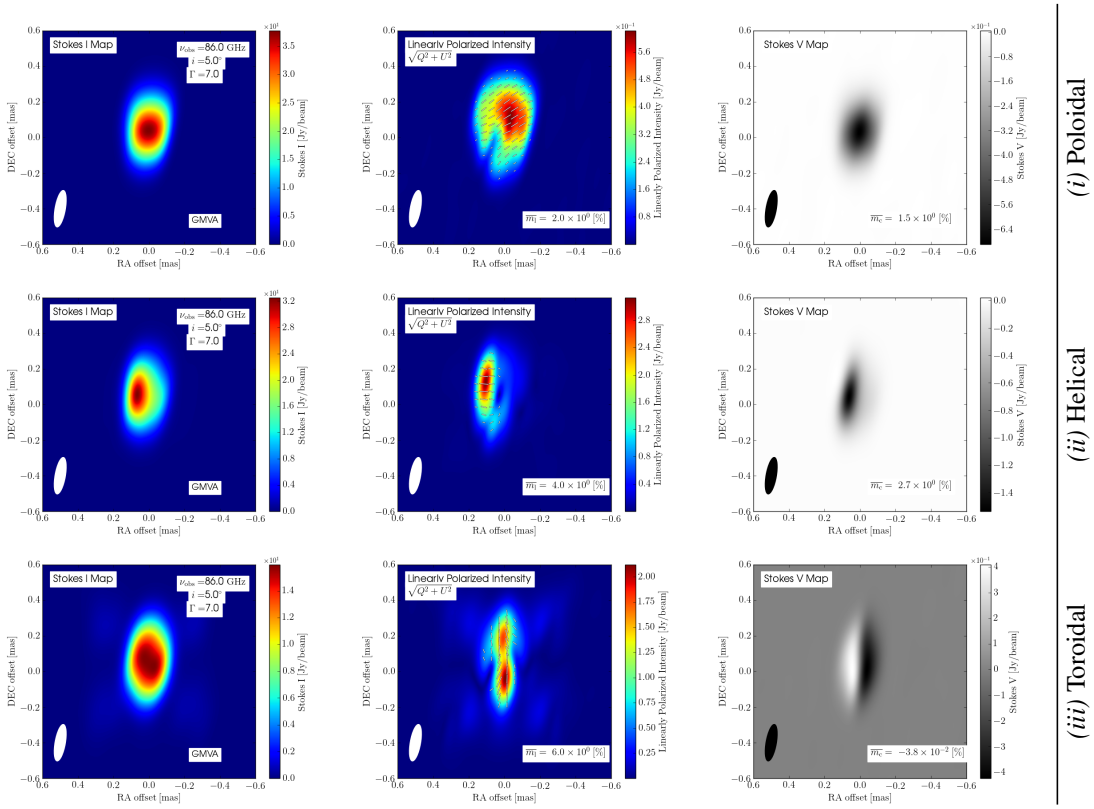


**Figure 5:** Ray-traced images of RMHD jet simulations in total intensity (left), linearly polarized intensity (middle), and circular polarization (right) when each jet is viewed edge-on to the jet-axis. The images highlight similar epochs in the jet's evolution of each 3D RMHD simulation at 86 GHz. The jet carries a purely poloidal magnetic field (top row), a helical magnetic field (middle row), and a purely toroidal magnetic field (bottom row). The ray-traced images are convolved with a Gaussian beam indicative of the resolution of the GMVA and with a Gaussian noise floor of $10^{-4}$ Jy/beam.

*toroidal magnetic field configuration within standing/recollimation shocks, and further, the bottom right panel in* (ii) *Fig. 5 highlights a clear switch in circular polarization from positive values to the left side of the blazar like simulation to negative values on the right side.*

## 5. Discussion

A wealth of new polarimetric data has been amassed of relativistic jets over the last decade, i.e., maps of AGN in both linearly polarized intensity and circular polarization, maps of Faraday rotation measure (RM) gradients along the jet, and analysis of EVPA orientation along the jet, all of which help to probe the underlying magnetic field geometry. In this section we make further comparisons between our ray-traced emission maps and observations to to further understand and interpret the different polarimetric features we observe in our simulations.

Faraday rotation measure (RM) gradients observed transverse to the jet axis hint at the existence of helical magnetic fields [e.g., in 0133+479, see 5, 8]. In a future work we plan to experiment with

generating synthetic RM maps of our three jet simulations to explore how robust RM is as a metric of the jet's internal magnetic field structure.

Helical/toroidal magnetic field morphologies have been invoked to explain an increase in linear polarization towards the edges of the jet [15, 23]. This edge brightened emission morphology is clearly seen in our simulations.

As discussed in [6], a purely toroidal magnetic field should result in symmetric edge brightened emission across the jet whereas, in contrast, a helical magnetic field should result in asymmetric emission along the jet edges. These distinct emission morphologies are present within our simulations (see, e.g., Fig. 3).

In our poloidal field simulation the jet spine/shock dominates the emission. This emission morphology has been observed in the jet of NGC 1052 [1]. In contrast, in the helical and toroidal field simulations the outer sheath is edge brightened and dominates the emission. This emission morphology has been observed in the jet of 3C 84 [see, e.g., 9, 13, 21].

Bi-modal EVPA patterns have been observed in a number of jets [20] in which the EVPAs preferentially align with the jet axis in the spine and, in contrast, appear predominantly perpendicular to the jet axis in the sheath. We see this bi-modal pattern in our toroidal field simulation (see, e.g., lower middle panel of Fig. 3).

The majority of blazars in which CP is detected tend to exhibit one sign/handedness of circular polarization [see, e.g., 11, 12]. A small number of sources, however, exhibit both negative and positive CP in the radio core region [see, e.g., 24]. As illustrated in the right column of Fig. 5, we find that a poloidal field produces only one sign of CP in the radio core whereas, in contrast, the the toroidal field produces both signs of CP in the core. This highlights the potential of combining linear and circular polarization maps to make a more robust determination of the magnetic field orientation within the jet.

## 6. Conclusion

We have carried out a systematic survey of full Stokes radiative transfer calculations exploring how: *(i)* the jet's magnetic field morphology and *(ii)* how various electron scaling relations effect the resultant linear and circular polarized emission.
In particular, we find:

- (Resolved) Circular polarization imaging has the potential to discriminate between a purely poloidal or a purely toroidal magnetic field morphology within the jet.

- When the jet is resolved (i.e., Fig. 3), toroidal magnetic fields result in edge-brightened jets whereas poloidal magnetic fields seem to highlight the jet's spine/recollimation shock.

- When the intrinsic magnetic field is purely toroidal in nature, the circular polarization exhibits a switch in sign.

- The EVPAs show a bi-modal scattering for the purely toroidal magnetic field configuration with the difference between the jet's spine and jet's sheath.

## References

[1] A.-K. Baczko. *Multi-Frequency VLBI Observations of the Active Galaxy NGC 1052*. PhD thesis, Max-Planck-Institute for Radioastronomy, July 2020.

[2] R. D. Blandford and D. G. Payne. Hydromagnetic flows from accretion disks and the production of radio jets. *Monthly Notices of the Royal Astronomical Society*, 199:883–903, June 1982. doi: 10.1093/mnras/199.4.883.

[3] R. D. Blandford and R. L. Znajek. Electromagnetic extraction of energy from Kerr black holes. *Monthly Notices of the Royal Astronomical Society: Letters*, 179:433–456, May 1977. doi: 10.1093/mnras/179.3.433.

[4] C. M. Fromm, M. Perucho, P. Mimica, and E. Ros. Spectral evolution of flaring blazars from numerical simulations. *Astronomy and Astrophysics*, 588:A101, Apr 2016. doi: 10.1051/0004-6361/201527139.

[5] D. Gabuzda. Determining the Jet Poloidal B Field and Black-Hole Rotation Directions in AGNs. *Galaxies*, 6(1):9, Jan. 2018. doi: 10.3390/galaxies6010009.

[6] D. C. Gabuzda. Magnetic fields in the relativistic jets of active galactic nuclei. *Proceedings of the International Astronomical Union*, 14(S342):189–196, 2018. doi: 10.1017/S1743921318007846.

[7] D. C. Gabuzda, V. M. Vitrishchak, M. Mahmud, and S. O'Sullivan. *Circular Polarization and Helical B Fields in AGN*, volume 386 of *Astronomical Society of the Pacific Conference Series*, page 444. 2008.

[8] D. C. Gabuzda, M. Nagle, and N. Roche. The jets of AGN as giant coaxial cables. *Astronomy and Astrophysics*, 612:A67, Apr. 2018. doi: 10.1051/0004-6361/201732136.

[9] G. Giovannini, T. Savolainen, M. Orienti, M. Nakamura, H. Nagai, M. Kino, M. Giroletti, K. Hada, G. Bruni, Y. Y. Kovalev, J. M. Anderson, F. D'Ammando, J. Hodgson, M. Honma, T. P. Krichbaum, S. S. Lee, R. Lico, M. M. Lisakov, A. P. Lobanov, L. Petrov, B. W. Sohn, K. V. Sokolovsky, P. A. Voitsik, J. A. Zensus, and S. Tingay. A wide and collimated radio jet in 3C84 on the scale of a few hundred gravitational radii. *Nature Astronomy*, 2:472–477, Apr 2018. doi: 10.1038/s41550-018-0431-2.

[10] P. Hardee, Y. Mizuno, and K.-I. Nishikawa. GRMHD/RMHD simulations and stability of magnetized spine-sheath relativistic jets. *Astrophysics and Space Science*, 311(1-3):281–286, Oct. 2007. doi: 10.1007/s10509-007-9529-1.

[11] D. C. Homan and M. L. Lister. MOJAVE: Monitoring of Jets in Active Galactic Nuclei with VLBA Experiments. II. First-Epoch 15 GHz Circular Polarization Results. *Astronomical Journal*, 131(3):1262–1279, Mar. 2006. doi: 10.1086/500256.

[12] D. C. Homan and J. F. C. Wardle. High Levels of Circularly Polarized Emission from the Radio Jet in NGC 1275 (3C 84). *Astrophysical Journal, Letters*, 602(1):L13–L16, Feb. 2004. doi: 10.1086/382273.

[13] J. Y. Kim, T. P. Krichbaum, A. P. Marscher, S. G. Jorstad, I. Agudo, C. Thum, J. A. Hodgson, N. R. MacDonald, E. Ros, R. S. Lu, M. Bremer, P. de Vicente, M. Lindqvist, S. Trippe, and J. A. Zensus. Spatially resolved origin of millimeter-wave linear polarization in the nuclear

region of 3C 84. *Astronomy an Astrophysics*, 622:A196, Feb. 2019. doi: 10.1051/0004-6361/201832920.

[14] J. A. Kramer and N. R. MacDonald. Ray-Tracing in Relativistic Jet Simulations: A Polarimetric Study of Magnetic Field Morphology and Electron Scaling Relations. *arXiv e-prints*, art. arXiv:2109.03514, Sept. 2021.

[15] M. Lyutikov, V. I. Pariev, and D. C. Gabuzda. Polarization and structure of relativistic parsec-scale AGN jets. *Monthly Notices of the Royal Astronomical Societ*, 360(3):869–891, July 2005. doi: 10.1111/j.1365-2966.2005.08954.x.

[16] N. R. MacDonald and A. P. Marscher. Faraday Conversion in Turbulent Blazar Jets. *Astrophysical Journal*, 862(1):58, July 2018. doi: 10.3847/1538-4357/aacc62.

[17] A. Mignone and G. Bodo. An HLLC Riemann solver for relativistic flows - II. Magnetohydrodynamics. *Monthly Notices of the Royal Astronomical Society*, 368(35):1040–1054, May 2006. doi: 10.1111/j.1365-2966.2006.10162.x.

[18] A. Mignone, G. Bodo, S. Massaglia, T. Matsakos, O. Tesileanu, C. Zanni, and A. Ferrari. PLUTO: A Numerical Code for Computational Astrophysics. *Astrophysical Journal Supplement*, 170(1):228–242, May 2007. doi: 10.1086/513316.

[19] K.-I. Nishikawa, Y. Mizuno, J. Gómez, I. Duţan, A. Meli, J. Niemiec, O. Kobzar, M. Pohl, H. Sol, N. MacDonald, and D. Hartmann. Relativistic Jet Simulations of the Weibel Instability in the Slab Model to Cylindrical Jets with Helical Magnetic Fields. *Galaxies*, 7(1):29, Jan 2019. doi: 10.3390/galaxies7010029.

[20] S. P. O'Sullivan and D. C. Gabuzda. Three-dimensional magnetic field structure of six parsec-scale active galactic nuclei jets. *Monthly Notices of the Royal Astronomical Societ*, 393(2): 429–456, Feb. 2009. doi: 10.1111/j.1365-2966.2008.14213.x.

[21] G. F. Paraschos, J. Y. Kim, T. P. Krichbaum, and J. A. Zensus. Pinpointing the jet apex of 3C 84. *Astronomy and Astrophysics*, 650:L18, June 2021. doi: 10.1051/0004-6361/202140776.

[22] O. Porth, C. Fendt, Z. Meliani, and B. Vaidya. Synchrotron Radiation of Self-collimating Relativistic Magnetohydrodynamic Jets. *Astrophysical Journal*, 737(1):42, Aug 2011. doi: 10.1088/0004-637X/737/1/42.

[23] A. B. Pushkarev, D. C. Gabuzda, Y. N. Vetukhnovskaya, and V. E. Yakimov. Spine-sheath polarization structures in four active galactic nuclei jets. *Monthly Notices of the Royal Astronomical Societ*, 356(3):859–871, Jan. 2005. doi: 10.1111/j.1365-2966.2004.08535.x.

[24] V. M. Vitrishchak, D. C. Gabuzda, J. C. Algaba, E. A. Rastorgueva, S. P. O'Sullivan, and A. O'Dowd. The 15-43 GHz parsec-scale circular polarization of 41 active galactic nuclei. *Monthly Notices of the Royal Astronomical Societ*, 391(1):124–135, Nov. 2008. doi: 10.1111/j.1365-2966.2008.13919.x.